Journal of Alloys and Compounds 509 (2011) 10105–10109

Contents lists available at ScienceDirect

Journal of Alloys and Compounds

journal homepage: www.elsevier.com/locate/jallcom

# N-doped $Sb_2Te$ phase change materials for higher data retention

Min Zhu[a,b,*], Liangcai Wu[a], Feng Rao[a], Zhitang Song[a], Xuelai Li[a,b], Cheng Peng[a], Xilin Zhou[a,b], Kun Ren[a,b], Dongning Yao[a], Songlin Feng[a]

[a] State Key Laboratory of Functional Materials for Informatics, Laboratory of Nanotechnology, Shanghai Institute of Micro-system and Information Technology, Chinese Academy of Sciences, 200050 Shanghai, China
[b] Graduate School of the Chinese Academy of Sciences, 100080 Beijing, China

ARTICLE INFO

*Article history:*
Received 18 June 2011
Received in revised form 8 August 2011
Accepted 10 August 2011
Available online 19 August 2011

*Keywords:*
Phase change memory
$Sb_2Te$
$Sb_2TeN$
Data retention

ABSTRACT

Crystallization temperatures of the $Sb_2Te$ films increase remarkably from 139.4 °C to 223.0 °C as the $N_2$ flow rates increasing from 0 sccm to 1.5 sccm. Electrical conduction activation energies for amorphous and crystalline states increase by doping nitrogen. A small amount of nitrogen atoms can locate at interstitial sites in the hexagonal structure, generating a strain field, and improving the thermal stability of amorphous state. The best 10-years lifetime at temperature up to 141 °C is found in $Sb_2TeN_1$ films. Doping excessively high nitrogen in $Sb_2Te$ film will form nitride and make Te separate out. As a result, the activation energy for crystallization decreases instead, accompanying with the deterioration of thermal stability. The power consumption of PCRAM test cell based on $Sb_2TeN_1$ film is ten times lower than that of PCRAM device using $Ge_2Sb_2Te_5$ films.



## 1. Introduction

Non-volatile memory (NVM) holds a significant position in semiconductor market, greatly profiting from the widespread application of flash memory chips in mobile phones and other portable electronic devices. Meanwhile, with rapid development of portable electronic devices, the requirements for NVM are raised: short erase, write and access times, low power consumption, high areal density and good durability. Therefore, many technologies are proposed to meet these requirements [1]. Compared with other competitors, phase change random access memory (PCRAM) may not excel in any category but still has an excellent all-round performance. PCRAM is based on the rapid reversible phase transition between amorphous and crystalline states of chalcogenide alloys, accompanying with large difference in electrical properties. Well-known chalcogenide alloys are $GeTe–Sb_2Te_3$ pseudobinary compounds and Sb–Te binary compounds. While $GeTe–Sb_2Te_3$ pseudobinary compounds possess a nucleation-dominated crystallization behavior, Sb–Te binary compounds exhibit a growth-dominated crystallization behavior, which lead to higher crystallization rate [2]. What is more, the crystallization rate can be further improved by higher Sb/Te atom ratio for Sb–Te binary compounds [3].

Similar with other Sb–Te-based materials, $Sb_2Te$, with a high-speed crystallization, however, exhibits low thermal stability [4]. The nitrogen-doping method is found to be one of the effective ways to solve this problem, which has been proved in N-doped GST [5,6] and $Sb_2Te_3$ films [7,8]. Therefore, in the study, nitrogen is added in $Sb_2Te$ films to boost the data retention performances.

## 2. Experiments

All films, 300-nm-thick, were deposited on $SiO_2$/Si (1 0 0) substrates by magnetron sputtering with alloy target. The background pressure and Ar/$N_2$ mixture gas pressure were $2.2 \times 10^{-4}$ and 0.25 Pa, respectively. The RF sputtering powers for $Sb_2Te$ and $Ge_2Sb_2Te_5$ targets were set to 20 W. Ar gas flow rate was 20 sccm. The nitrogen contents were controlled by changing $N_2$ gas flow rates from 0 sccm to 1.5 sccm. The thickness of the films was measured by scanning electron microscope (SEM). The composition of the films was determined using energy dispersion X-ray spectrometry (EDS). Structures of the films annealed at various temperatures under the protection of Ar atmosphere were investigated by X-ray diffraction (XRD). The diffraction patterns were taken in the $2\theta$ range from 10° to 68° with Cu Kα radiation (λ = 1.54056 Å). The variations of sheet resistances of the films with the increasing temperature are measured in a homemade vacuum chamber at different heating rates. The resistance–voltage and endurance performances were measured by Keithley 2600m and Agilent-81104A parameter analyzer.

## 3. Results and discussion

Fig. 1(a) shows the sheet resistance as a function of temperature ($R$–$T$) at a heating rate of 20 °C/min for $Sb_2Te$ and N-doped $Sb_2Te$ films. The sheet resistance of as-deposited $Sb_2Te$ film is $3.8 \times 10^5$ Ω/Sq, and then falls slowly with increasing temperature until a sudden drop occurs around 139 °C, corresponding to

* Corresponding author at: State Key Laboratory of Functional Materials for Informatics, Laboratory of Nanotechnology, Shanghai Institute of Micro-system and Information Technology, Chinese Academy of Sciences, 200050 Shanghai, China.
*E-mail address:* minzhu@mail.sim.ac.cn (M. Zhu).

0925-8388/$ – see front matter © 2011 Elsevier B.V. All rights reserved.
doi:10.1016/j.jallcom.2011.08.050

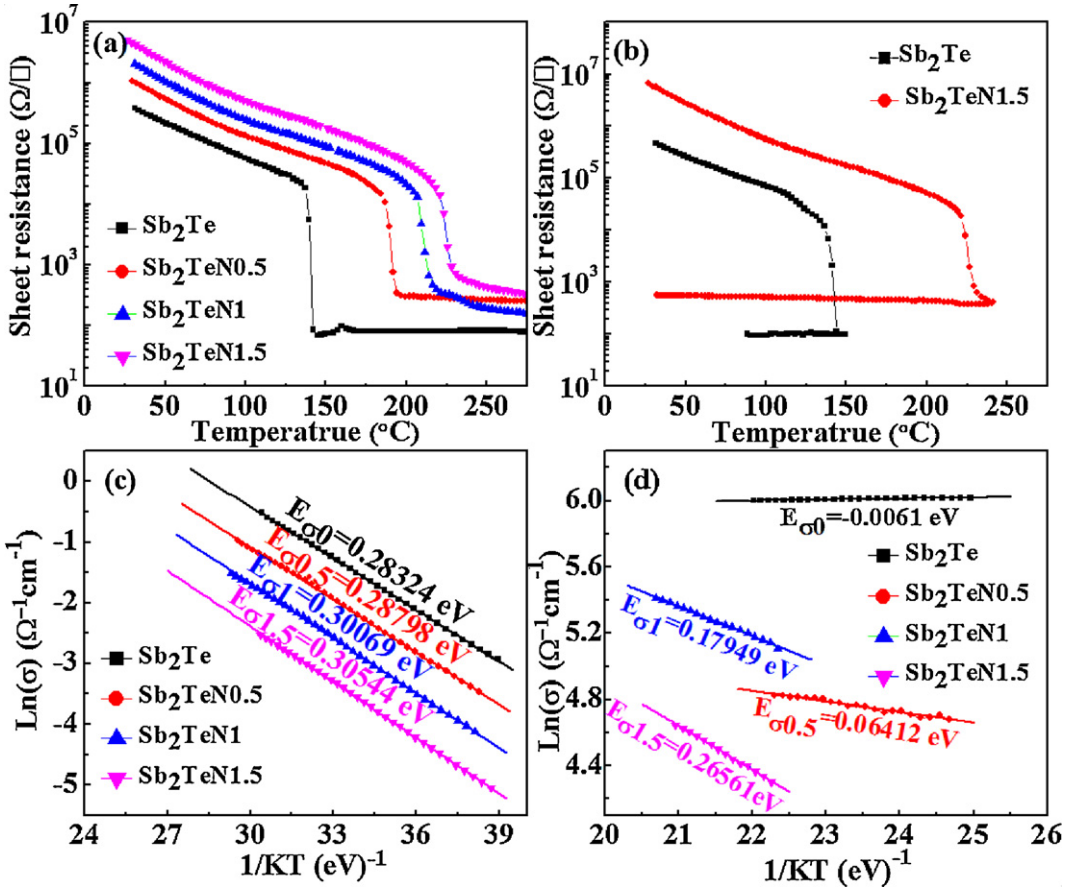


**Fig. 1.** (a) Sheet resistance as a function of temperature ($R$–$T$) at a heating rate of 20 °C/min for $Sb_2Te$ and N-doped $Sb_2Te$ films. (b) Temperature dependence of the sheet resistance for $Sb_2Te$ and $Sb_2TeN_{1.5}$ films. Arrhenius plots of ln($\sigma$) versus 1/$KT$ for (c) amorphous and (d) crystalline $Sb_2Te$ and N-doped $Sb_2Te$ films.

crystallization temperature ($T_c$) of $Sb_2Te$ films. In this experiment, $T_c$ of $Ge_2Sb_2Te_5$ (GST) films is 168.8 °C (not shown), which is a little higher than the result reported (150 °C) [9]. The slight stoichiometry deviation of GST may be responsible for the difference. Only one rapid drop occurs in $Sb_2Te$ film, which indicates that $Sb_2Te$ film just has the crystallization process without the phase transition between different crystalline phases. It will be proved by XRD in Fig. 2(a). After the addition of $N_2$ gas, the sheet resistances and the $T_c$ of $Sb_2Te$ films increase sharply. The $T_c$ of $Sb_2TeN0.5$, $Sb_2TeN1$ and $Sb_2TeN1.5$ films are 186.8 °C, 209.1 °C and 223.0 °C, respectively. Nitrogen atoms may locate at interstitial sites of $Sb_2Te$, and distort the crystal structure, which may generate a strain field and lead to a higher crystallization temperature [5]. In addition, as the temperature further increases, the change tendencies of sheet resistance

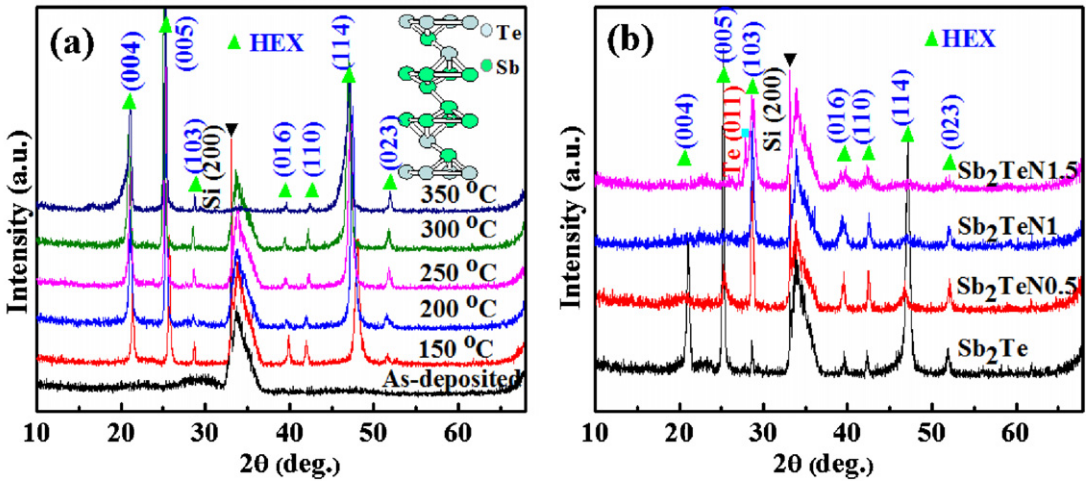


**Fig. 2.** XRD patterns of (a) $Sb_2Te$ films annealed at several temperatures and (b) $Sb_2TeN$ films with different $N_2$ flow rates annealed at 300 °C. The inset shows the structure of $Sb_2Te$.

seem to be different when sheet resistances of $Sb_2Te$ and $Sb_2TeN_{0.5}$ films reach a steady value, that of $Sb_2TeN_1$ and $Sb_2TeN_{1.5}$ films continuous decline.

In order to find out the reasons for this discrepancy, $Sb_2Te$ and $Sb_2TeN_{1.5}$ films were heated above $T_c$ and subsequently cooled at the same rate ($\alpha = 20\,^{\circ}C/min$), as shown in Fig. 1(b). The sheet resistance differences between $Sb_2Te$ and $Sb_2TeN_{1.5}$ films are largest. This is why these two films are selected. In Fig. 1(b), the $R$–$T$ curve of $Sb_2Te$ films shows a positive slope during cooing [$(dR/dT) > 0$], which presents metallic characteristic. However, a negative slope is observed in that of $Sb_2TeN_{1.5}$ films, which exhibits the characteristic of semiconducting film [10]. Thus, it is can be concluded that the band-gap widths of crystalline $Sb_2Te$ films is increased by doping nitrogen, which leads to above discrepancy.

Fig. 1(c and d) show the conductivity of amorphous and crystalline films as a function of the reciprocal temperature. Conductivity ($\sigma$) can be obtained using the equation: $\sigma = 1/dR_{sq}$, where $d$ is the thickness of films and $R_{sq}$ is the sheet resistance of films, which can be extracted from Fig. 1(a). The electrical conduction activation energies in amorphous/crystalline layer ($E_{\sigma a}/E_{\sigma c}$) are related to the conductivity by the Arrhenius equation: $\sigma = \sigma_0 \exp(-E_\sigma/KT)$, where $\sigma_0$ is a pre-exponential factor, $E_\sigma$ the activation energy for conduction in amorphous or crystalline layer, $K$ the Boltzmann constant and $T$ is the absolute temperature [11]. The $E_{\sigma a}$ increase monotonously from 0.28324 eV to 0.30544 eV as $N_2$ gas flow rates increasing from 0 to 1.5 sccm. The $E_{\sigma a}$ value is about half of the band-gap value for amorphous film [12]. Therefore, the band-gap width of the amorphous $Sb_2Te$ film is gradual extended with the increase of $N_2$ flow rate as well. Besides, $E_{\sigma c}$ increase from −0.0061 eV of pure $Sb_2Te$ film to 0.26561 eV for $Sb_2TeN_{1.5}$ film.

The results of $R$–$T$ plots, mentioned above, show that only one phase transformation occurs in the $Sb_2Te$ and N-doped $Sb_2Te$ films, so XRD is applied to confirm it. Fig. 2(a) shows the XRD results of pure $Sb_2Te$ films annealed at different temperatures. In Fig. 2(a), the crystalline peaks of HEX phase first appear at 150 °C. The lattice parameters are calculated as $a = 4.2661$ nm and $c = 17.631$ nm ($P\bar{3}m1$), which is in good agreement with other report [13]. No other structure transformation takes place with the rise of annealing temperature, corresponding well with the sheet resistance change. Fig. 2(b) shows the XRD patterns for $Sb_2Te$ films with different $N_2$ flow rates annealed at 300 °C for 5 min. In spite of different doping nitrogen contents, all films show HEX structure as well. The comparison between the pure $Sb_2Te$ films and N-doped $Sb_2Te$ films shows an increase in the intensity of the (1 0 3) peak and a decrease in that of the (0 0 4) and (0 0 5) peaks. The diffraction peaks of N-doped $Sb_2Te$ films become broaden as the nitrogen flow rates increase. The grain size, estimated by Scherer's equation, is effectively restrained by implanting nitrogen. Similar behaviors are also found in the case of the N-doped GST films [5]. The small grain size may induce more grain boundaries and more carrier scattering [8], which is one of the reasons why the sheet resistance of N-doped $Sb_2Te$ film enhances with increasing nitrogen flow rate. Special attention should be paid to the (0 1 1) diffraction peak for $Sb_2TeN_{1.5}$ film, belonging to tellurium. Nevertheless, the diffraction peak is not observed in other films, which demonstrates that Te separates from $Sb_2Te$ when the doping $N_2$ is overflow. Agafonov et al. [13] showed that the structure of $Sb_2Te$ consists of nine layers stacked along the $c$-axis and presents the combination of five-layer stacks of $Sb_2Te_3$ and two-layer stacks of $Sb_2$. When a small amount of nitrogen is doped into $Sb_2Te$ film, nitrogen atoms can locate at interstitial sites in the HEX structure. However, owing to excessively high $N_2$ flow rate, SbN begins to form, as a result, Te from $Sb_2Te$ films separates out [7].

Fig. 3 shows the Kissinger plots of GST [12], $Sb_2Te$ and N-doped $Sb_2Te$ films. The crystallization temperatures of the films are

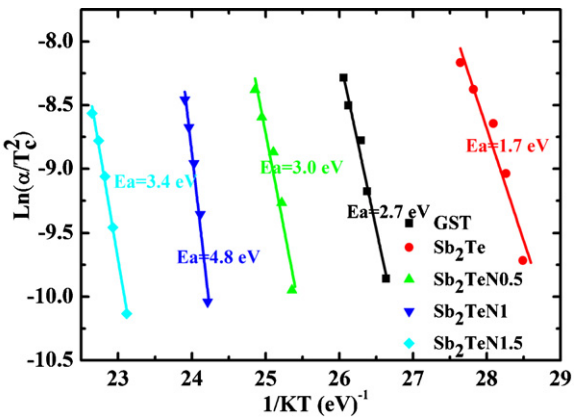


**Fig. 3.** The Kissinger plots ($\ln(\alpha/T_c^2)$ *vs* $1/KT$ of GST, $Sb_2Te$ and N-doped $Sb_2Te$ films.

obtained from the $R$–$T$ plots with the heating rate from 10 °C/min to 50 °C/min. The crystallization activation energy, $E_a$, for the transformation from amorphous phase to crystalline phase, can be get from the slope of the Kissinger plots ($\ln(\alpha/T_c^2)$ *vs* $1/KT$). In this experiment, the $E_a$ of GST films is determined to be $2.7 \pm 0.19$ eV. $E_a$ of $Sb_2Te$ films increase from $1.7 \pm 0.19$ eV to $4.8 \pm 0.3$ eV with the $N_2$ flow rates increasing from 0 to 1 sccm. Although the $N_2$ flow rate increases to 1.5 sccm, the $E_a$ unexpectedly decreases to $3.4 \pm 0.13$ eV. The same trend of $E_a$ is found in Fig. 4, in which $E_a$ can be obtained from the slope of failure time versus reciprocal temperature ($1/KT$) using the Arrhenius equation [14].

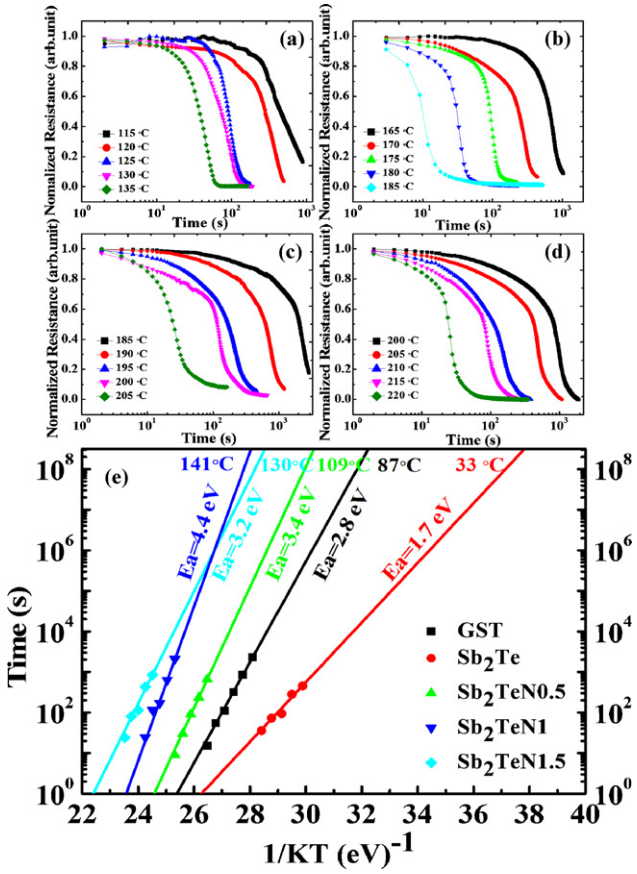


**Fig. 4.** The curves of sheet resistance versus time at various isothermal annealing temperatures for (a) $Sb_2Te$, (b) $Sb_2TeN_{0.5}$, (c) $Sb_2TeN_1$ and (d) $Sb_2TeN_{1.5}$ films. (e) Arrhenius plots of data retention showing extrapolated temperature for 10-years data retention.

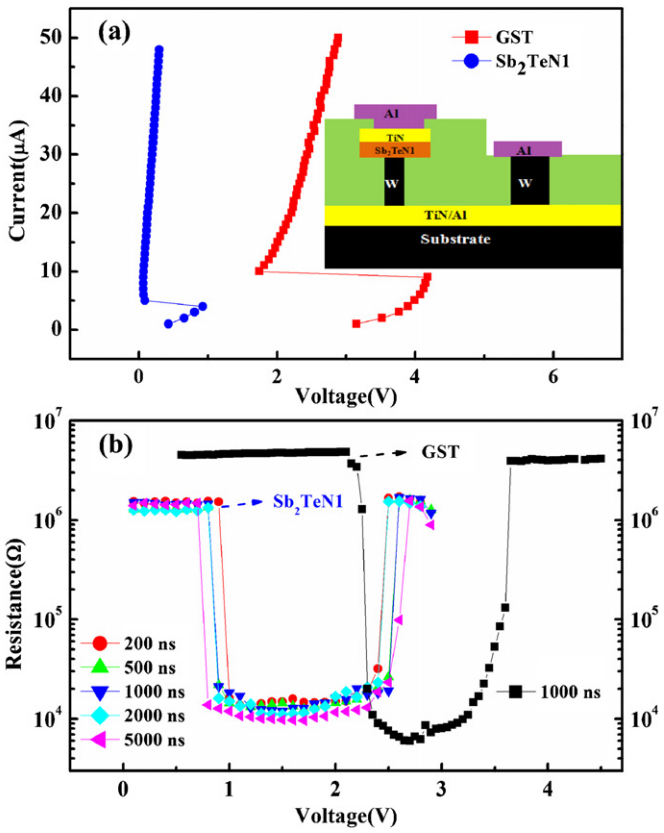


**Fig. 5.** (a) Current–voltage characteristics of PCRAM test cell devices fabricated with $Sb_2TeN_1$ and GST films. The inset shows the schematic diagram of the PCRAM cell structure. (b) Resistance–voltage characteristics of the devices based on $Sb_2TeN_1$ and GST films.

Furthermore, the values of $E_a$ of all films obtained from both methods are very close.

The curves of sheet resistance versus time at various isothermal annealing temperatures for (a) $Sb_2Te$, (b) $Sb_2TeN_{0.5}$, (c) $Sb_2TeN_1$ and (d) $Sb_2TeN_{1.5}$, as shown in Fig. 4. The failure time is defined as the time when the sheet resistance of the film decreases to half of the initial value. According to the Arrhenius equation [14], basing on the failure time gets from Fig. 4 (b–d), extrapolated temperatures of all films for 10-years data retention are included in Fig. 4 (e). The 10-years lifetime for pure $Sb_2Te$ films, only 33 °C, indicates that pure $Sb_2Te$ film is not suitable for application in phase change device. Data retention of N-doped $Sb_2Te$ films, compared with that of pure $Sb_2Te$ film, is improved remarkably. The highest 10-years lifetime, 141 °C, is obtained in $Sb_2TeN_1$ film, which is already sufficient to apply in automobile electronics (120 °C for 10-years) [15]. As the $N_2$ flow rate increases to 1.5 sccm, the 10-years lifetime decreases to 130 °C instead. The weaker data retention of $Sb_2TeN_{1.5}$ film, compared with $Sb_2TeN_1$ films, may due to the lower value of $E_a$, which has been mentioned above. This is because that the crystallization process needs to overcome the crystallization activation energy [16], thus low $E_a$ implies poor reliability of amorphous phase. As mentioned above, doping excessively high $N_2$ flow rate (1.5 sccm) leads to the formation of SbN and the separation of Te from $Sb_2Te$ films. Besides, as the atom ratio of Sb and Te lower than 2:1, the thermal strbility of Sb-Te alloy first improves with the rise of Sb content [17]. Consequently, the separation of Te and the remarkable reduction of Sb in $Sb_2TeN_{1.5}$ film are perhaps responsible for the diminution of crysatllization activation energy and the deterioration of thermal stability.

Possessing the best data retention in this study, $Sb_2TeN_1$ film was applied in the PCRAM test cell to study its electrical behavior. After all, a phase change material, which is sufficient for most consumer applications and automotive applications, is not only of good thermal stability but also with low power consumption and distinct resistance discrepancy between crystalline state (Set) and amorphous state (Reset). PCRAM test cell with a tungsten-heating electrode 260 nm in diameter has been fabricated using 0.18 μm COMS technology. The schematic diagram of the PCRAM cell structure is shown in the inset of Fig. 5(a). Fig. 5(a) shows current–voltage ($I$–$V$) characteristics of PCRAM test cell fabricated with $Sb_2TeN_1$ and GST films. Initially, only a negligible current flows through the cell because of the high initial resistance of amorphous state. The $I$–$V$ curve does snap back when the applied voltage beyond the threshold voltage, which indicates that the phase transition from amorphous state to crystalline phase. The threshold voltage for $Sb_2TeN_1$ device is only 0.92 V, when 4.18 V for GST device.

Fig. 5(b) shows resistance–voltage ($R$–$V$) plots of the PCRAM cell based on GST and $Sb_2TeN_1$ films. In the case of $Sb_2TeN_1$ device, the resistance ratio between Reset and Set state is about two orders of magnitude. Most obviously, 0.9 V and 2.5 V can achieve Set and Reset operations, respectively. Furthermore, the threshold voltages are hardly changed with the increasing voltage pulse widths. The required dissipated energy for the Reset operation can be estimated using the equation $(V_{Reset}^2/R_{Set}) \times t_{Reset}$. At the condition of the same $t_{Reset}$ (1000 ns), the power consumption for the Reset operation of $Sb_2TeN_1$ device is calculated to be around $3.0 \times 10^{-10}$ J, which is ten times lower than that of GST device.

## 4. Conclusions

Phase change abilities of $Sb_2Te$ and N-doped $Sb_2Te$ phase change materials were systemically investigated. XRD results show that crystalline $Sb_2Te$ and N-deposited $Sb_2Te$ films have HEX structure. The crystallization temperatures for $Sb_2Te$, $Sb_2TeN_{0.5}$, $Sb_2TeN_1$ and $Sb_2TeN_{1.5}$ films are 139.4 °C, 186.8 °C, 209.1 °C and 223.0 °C, respectively. The band-gap widths of the amorphous and crystalline $Sb_2Te$ films are gradual extended with increasing $N_2$ flow rate. The crystallization activation energies of N-doped $Sb_2Te$ films increase first, and then decrease. The data retention shows the similar trend and the maximum temperature for 10-years lifetime, 141 °C, is found in $Sb_2TeN_1$ films. The PCRAM cells based on $Sb_2TeN_1$ films have the advantage of low power consumption, and the threshold voltages for Set and Reset operations are only 0.9 V and 2.5 V, respectively. To sum up, we recommend $Sb_2TeN_1$ as a good candidate for PCRAM application.

## Acknowledgements

Financial support by the National Integrated Circuit Research Program of China (2009ZX02023-003), the National Basic Research Program of China (2010CB934300, 2011CB309602, 2011CB932800), the National Natural Science Foundation of China (60906004, 60906003, 61006087, 61076121), and the Science and Technology Council of Shanghai (09QH1402600, 1052nm07000).

## References

[1] M. Wuttig, N. Yamada, Nat. Mater. 6 (2007) 824.
[2] L. van Pieterson, M.H.R. Lankhorst, M. van Schijndel, A.E.T. Kuiper, J.H.J. Roosen, J. Appl. Phys. 97 (2005) 083520.
[3] M.H.R. Lankhorst, L. van Pieterson, M. van Schijndel, B.A.J. Jacobs, J.C.N. Rijpers, Jpn. J. Appl. Phys. 42 (Part 1) (2003) 863.
[4] K.-F. Kao, H.-Y. Cheng, C.-M. Lee, T.-S. Chin, IEEE Trans. Magn. 43 (2007) 927.
[5] T.H. Jeong, M.R. Kim, H. Seo, J.W. Park, C. Yeon, Jpn. J. Appl. Phys. 39 (Part 1) (2000) 2775.

[6] B. Liu, T. Zhang, J.L. Xia, Z.T. Song, S.L. Feng, B. Chen, Semicond. Sci. Technol. 19 (2004) L61.
[7] Y. Yin, H. Sone, S. Hosaka, J. Appl. Phys. 102 (2007) 064503.
[8] C.Z. Wang, J.W. Zhai, S.Y. Bai, X. Yao, Mater. Lett. 64 (2010) 2314.
[9] I. Friedrich, V. Weidenhof, W. Njoroge, P. Franz, M. Wuttig, J. Appl. Phys. 87 (2000) 4130.
[10] T. Siegrist, P. Jost, H. Volker, M. Woda, P. Merkelbach, C. Schlockermann, M. Wuttig, Nat. Mater. 10 (2011) 202.
[11] Y. Zhang, J. Feng, Z.F. Zhang, B.C. Cai, Y.Y. Lin, T.A. Tang, B. Chen, Appl. Surf. Sci. 254 (2008) 5602.
[12] S. Privitera, E. Rimini, R. Zonca, Appl. Phys. Lett. 85 (2004) 3044.
[13] V. Agafonov, N. Rodier, R. Ceolin, R. Bellissent, C. Bergman, J.P. Gaspard, Acta Crystallogr. Sect. C: Cryst. Struct. Commun. 47 (1991) 1141.
[14] F. Rao, Z. Song, K. Ren, X. Zhou, Y. Cheng, L. Wu, B. Liu, Nanotechnology 22 (2011) 145702.
[15] K.-F. Kao, C.-M. Lee, M.-J. Chen, M.-J. Tsai, T.-S. Chin, Adv. Mater. 21 (2009) 1695.
[16] S.W. Ryu, J.H. Oh, J.H. Lee, B.J. Choi, W. Kim, S.K. Hong, C.S. Hwang, H.J. Kim, Appl. Phys. Lett. 92 (2008) 142110.
[17] C.W. Sun, J.Y. Lee, M. Youm, Y.T. Kim, Phys. Status Solidi 1 (2007) R25.